
This is an electronic reprint of the original article.
This reprint may differ from the original in pagination and typographic detail.

Malitckii, E.; Remes, H.; Lehto, P.; Yagodzinskyy, Y.; Bossuyt, S.; Hänninen, H.

Strain accumulation during microstructurally small fatigue crack propagation in bcc Fe-Cr ferritic stainless steel

Published in:
Acta Materialia

DOI:
[10.1016/j.actamat.2017.10.038](https://doi.org/10.1016/j.actamat.2017.10.038)

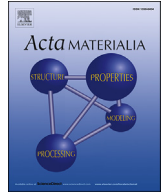
Published: 01/02/2018

Document Version
Publisher's PDF, also known as Version of record

Published under the following license:
CC BY-NC-ND

Please cite the original version:
Malitckii, E., Remes, H., Lehto, P., Yagodzinskyy, Y., Bossuyt, S., & Hänninen, H. (2018). Strain accumulation during microstructurally small fatigue crack propagation in bcc Fe-Cr ferritic stainless steel. *Acta Materialia*, 144, 51-59. <https://doi.org/10.1016/j.actamat.2017.10.038>

This material is protected by copyright and other intellectual property rights, and duplication or sale of all or part of any of the repository collections is not permitted, except that material may be duplicated by you for your research use or educational purposes in electronic or print form. You must obtain permission for any other use. Electronic or print copies may not be offered, whether for sale or otherwise to anyone who is not an authorised user.



Full length article

Strain accumulation during microstructurally small fatigue crack propagation in bcc Fe-Cr ferritic stainless steel



E. Malitckii*, H. Remes, P. Lehto, Y. Yagodzinskyy, S. Bossuyt, H. Hänninen

Aalto University School of Engineering, Department of Mechanical Engineering, Espoo, Finland

ARTICLE INFO

Article history:

Received 12 July 2017

Received in revised form

25 September 2017

Accepted 16 October 2017

Available online 23 October 2017

Keywords:

Microstructurally small fatigue crack

Digital image correlation

Shear strain localization

bcc crystal structure

ABSTRACT

Strain accumulation was studied by digital image correlation technique (DIC) during microstructurally small fatigue crack propagation in polycrystalline 18%Cr ferritic stainless steel. Load-controlled fatigue testing was performed with R-ratio of 0.1 and frequency 10 Hz. The maximum applied stress was well below the yield stress of the studied material. The effect of the observed strain field on crack growth rate variation is discussed. Fracture surfaces were studied by scanning electron microscopy (SEM) evidencing the connection between the mechanism of the fatigue crack growth, accumulated strain and crack growth rate. Detailed study of fracture surface morphology was carried out by atomic force microscopy (AFM). Results indicate two processes of material damage accumulation and failure during cyclic loading: 1) local shear strain zones form successively ahead of the crack tip, and 2) fatigue crack growth occurs by both single- and multiple-slip mechanisms. The place and intensity of shear strain localization zones vary during the crack growth that is related closely to the local variation of crack growth rate.

© 2017 Acta Materialia Inc. Published by Elsevier Ltd. This is an open access article under the CC BY-NC-ND license (<http://creativecommons.org/licenses/by-nc-nd/4.0/>).

1. Introduction

Investigation of the fatigue properties of the structural materials in microstructural level increases the reliability of fatigue crack growth predictions and allows prevention of the fatigue failures of the structural components leading possibly to catastrophic industrial or civil accidents. Fatigue crack growth rate has been extensively studied for decades in materials of different microstructures evidencing some common features of the crack propagation behavior.

A two-stage process of fatigue crack was first documented by Forsyth and observed in a variety of ferrous, titanium and aluminum alloys [1]. Stage I crack growth occurs along the single crystallographic slip band and is dominated by shear. Stage II crack growth is associated with crack propagation on a plane normal to the applied stress direction involving simultaneous or alternating plastic flow along two slip systems forming striations on the fracture surface [1–5]. The observed crack behavior in Stage II is connected to two mechanisms of fatigue crack growth: ductility exhaustion and plastic blunting. In ductility exhaustion mechanism, the fatigue crack grows as a result of damage accumulation

ahead of the crack tip, in the materials that exhibit planar slip. In plastic blunting mechanism, the fatigue crack grows by the deformation process that occurs within the slip planes at the angle to the crack tip. Blunting occurs at the crack tip during loading and subsequent re-sharpening during unloading of the material [6]. It is well-known that a long or large crack is associated to Stage II cracking. The consideration of short or small cracks is more challenging. Tokaji et al. classified small cracks as microstructurally, mechanically, and physically small cracks [14–16]. They reported that the mechanically and physically small cracks propagate mainly by Stage II mechanism with a little influence of microstructure. In the case of microstructurally and mechanically small crack growth, Stage I mechanism and the anomalous crack growth including Stage I and II mechanism was observed. The physical reasons causing this anomalous crack growth behavior are not well known.

With the aim to predict the fatigue crack growth in the materials phenomenological relationships were discovered between the crack growth rate and fatigue loading parameters by developing the computational mechanisms for the crack growth modeling [7–10], such as linear elastic fracture mechanics (LEFM) based on Paris law or dislocation modeling. However, modeling considers often the material properties through empirical constants for the better correlation with the experimental data. While the LEFM can be effectively used for the modeling of the propagation of large fatigue cracks, the small fatigue crack growth rate modeling needs a

* Corresponding author.

E-mail address: evgeny.malitckiy@aalto.fi (E. Malitckii).

deeper understanding of the fracture mechanisms. It is assumed that the growth of the small fatigue cracks is driven by shear and is dominated by local plasticity [8,9,11]. At the same time, the microstructural features such as grain boundaries, grain size and grain orientation as well as the sample geometry influence the small fatigue crack growth. A number of experimental studies show that the small fatigue cracks grow along the preferred slip planes [12,13]. Long-term simulation using dislocation modeling techniques shows that the small fatigue crack propagation is accompanied with the formation of the local plastic zone ahead of the crack tip [8,9].

Although several theoretical models exist for a small fatigue crack, limited amount of experimental studies have been performed for clarification of the material behavior during fatigue crack growth at the grain size level. Such investigations can be effectively made by digital image correlation (DIC) for small fatigue cracks in coarse-grained materials. In some of the previous studies, DIC techniques have been related to investigation of the strain field distribution accompanied with the long fatigue crack propagation [17,18]. Others consist of the strain measurements during a small amount of fatigue cycles using *ex-situ* DIC methods that blur over the details of the development of the strain field. The present research is focused on the investigation of accumulated plastic strain that results in a microstructurally small fatigue crack in 18% Cr ferritic stainless steel. Full-field investigation takes into consideration the connection of the strain field distribution, microstructure, crack growth rate, crack path and fracture behavior that provides unique knowledge of the small fatigue crack growth mechanism in a polycrystalline alloy with body-centered cubic (bcc) crystal structure. Such an experimental procedure and obtained results provide additional knowledge for an appropriate prediction of the small fatigue crack propagation also in other polycrystalline alloys.

2. Experimental

Ferritic stainless steel (ASTM UNS S43940) with 18% chromium was provided by Outokumpu Stainless Oyj in the shape of hot-rolled plate with a thickness of 3 mm. The chemical composition of the studied steel is shown in Table 1.

The steel plate was annealed in nitrogen atmosphere at temperature of 1200 °C for 1 h and quenched in water. Grain size (GS) measurement was performed from optical microscopy photographs using the intercept length method [19]. The annealing procedure results in an increase of the average grain size of the studied steel up to 349 μm without extensive formation of chromium carbides [20].

The notched tensile specimens with thickness of 1 mm were cut from the annealed plate of the studied steel using electrical discharge machining as shown schematically in Fig. 1. Surfaces of the specimens were polished finishing with 0.02 μm colloidal silica vibratory polishing that is acceptable for EBSD analysis.

Initial cracks with length from 1 μm to 20 μm were produced at the notch tip using a servo-hydraulic MTS loading unit where the specimen was subjected to uniaxial cyclic loading ($\sigma_{\min} = -50$ MPa, $\sigma_{\max} = 300$ MPa), *R*-ratio -0.16 , and fatigue frequency 10 Hz. Number of cycles needed to produce the initial crack was found to be about 10,000. Worth to note is that the fatigue loading with a

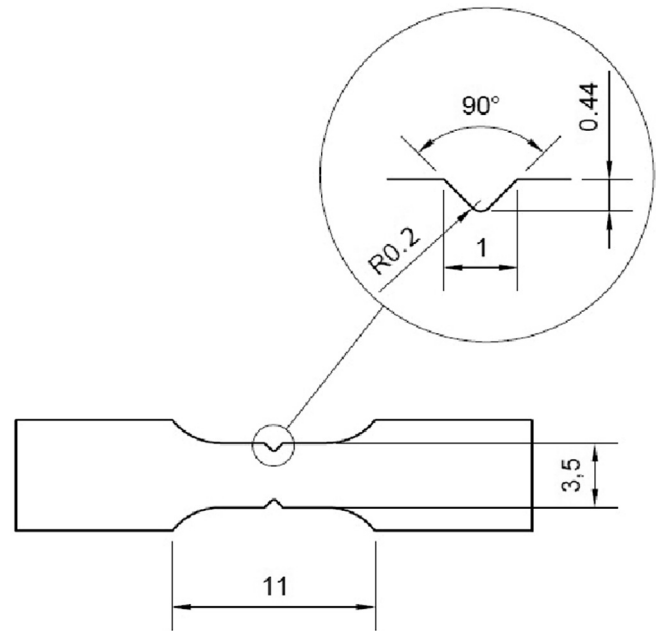


Fig. 1. Schematic view of the fatigue test specimen of the studied ferritic stainless steel.

positive *R*-ratio did not result in the fatigue crack initiation even after 100,000 cycles. The microstructure of the steel was studied from the side surface of the specimen in the vicinity of the notches using the EBSD analysis. Characteristic size of the studied area is about 0.9×1.2 mm.

Load-controlled fatigue testing of the pre-cracked specimens was carried out using *R*-ratio of 0.1 ($\sigma_{\min} = 35$ MPa, $\sigma_{\max} = 350$ MPa) and fatigue frequency 10 Hz. The maximum applied stress was chosen to be about 365 MPa, that is less than the yield stress measured in CERT with a strain rate of $2 \times 10^{-3} \text{ s}^{-1}$ (see Fig. 2a). During the fatigue testing the elongation of the specimen was measured as shown in Fig. 2b. Elongation of the specimen decreases reaching a saturation value from 100 k cycles. Then, the elongation increases steeply after about 160 k cycles. This transient phenomenon is associated with cyclic strain hardening and subsequent fatigue crack opening before final fracture.

Fatigue testing was accompanied with digital image correlation (DIC) measurement performed over the notched area of the specimen shown by circle in Fig. 1. This area was observed using an optical microscope, 16X Precision Zoom Lens, with a resolution of 2 μm/pixel. The characteristic size of the speckle pattern required for DIC calculations is about 10 μm [21]. Images were captured during the temporary (10 s) stops of the fatigue test after each 500 cycles at an average stress of about 210 MPa. The frame captured after the first 500 cycles was chosen to be the reference frame for the digital image correlation. Thus, only an increment of plastic deformation caused by the cyclic loading was analyzed. DIC calculation was performed using a commercial LaVision software (DaVis 8.3.1).

The region of interest is the notched area shown in Fig. 3. Vickers microindentation marks were used to specify the area for proper alignment of the strain field calculated by DIC and electron

Table 1
Chemical composition of ASTM UNS S43940 ferritic stainless steel, wt.%.

C	Si	Mn	P	Cr	Mo	Nb	Ni	Ti	Cu	Al	As	Co	Sn	V	W
0.014	0.61	0.42	0.03	17.7	0.024	0.393	0.18	0.138	0.118	0.025	0.007	0.0183	0.007	0.055	0.037

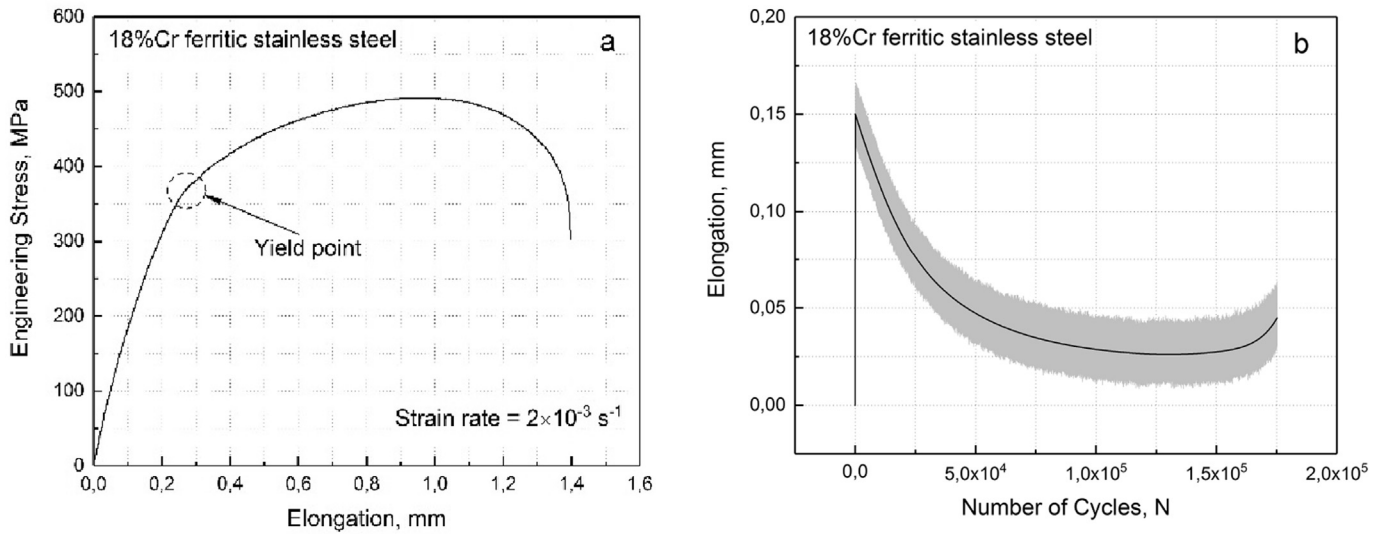


Fig. 2. CERT stress-strain curve of the annealed tensile specimen of ASTM UNS S43940 ferritic stainless steel (a). Change of elongation during the load-controlled fatigue test of the pre-cracked specimen of the ferritic stainless steel (b).

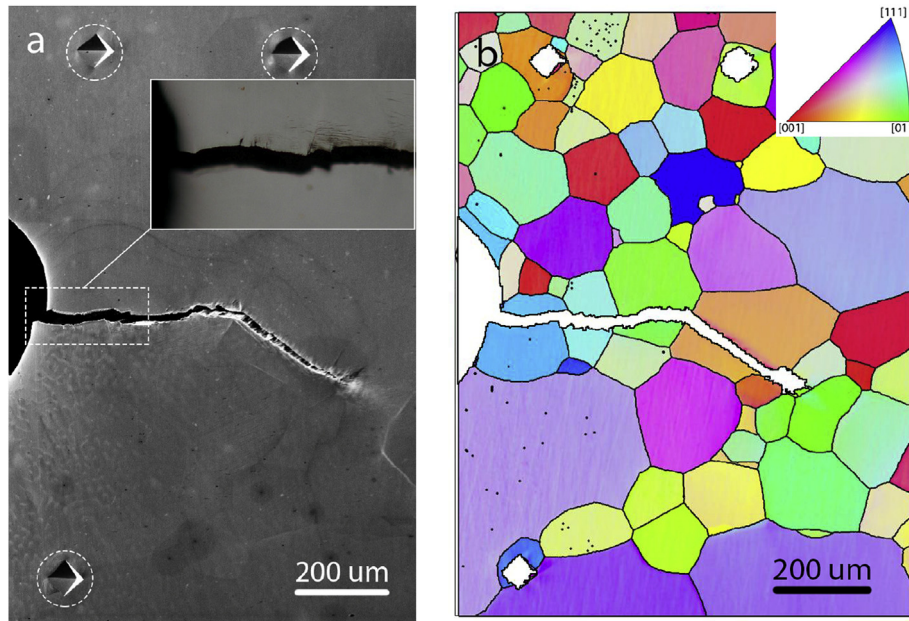


Fig. 3. Micrograph of the side surface of the specimen in the vicinity of the notch after a fatigue test (a) and the inverse pole figure (IPF) map of the same area with IPF key in the insert (b) of the ferritic stainless steel specimen. Microindentation marks shown by dashed circles are used for the proper alignment of DIC strain field and EBSD images.

backscatter diffraction (EBSD) images. Fractography was performed for the fracture surfaces of the specimens tested in fatigue using Zeiss Ultra 55 FEG-SEM. Atomic force microscopy (AFM) was performed for the fracture surfaces of the specimens using a Veeco Dimension 5000 microscope.

3. Results

Small fatigue crack propagates transgranularly in the plane normal to the applied stress while the specimen is subjected to macroscopically elastic deformation (see Fig. 3). The damage zone is localized within the grains of the crack propagation path. With fatigue crack growth and subsequent reduction of the specimen cross-section area the amount of plastic deformation increases

resulting in change of the crack path direction. Microstructure characterization using EBSD analysis reveals that the fatigue crack propagates through the three first neighboring grains without an obvious relation to their orientation.

Crack growth rate was analyzed by optical microscopy on the side surface of the specimen during the fatigue loading. Fig. 4a shows the measured crack length versus the number of loading cycles. Crack length changes irregularly with increase of the amount of cyclic loadings that evidences the retardation of the crack growth rate. Crack growth rate was calculated from spline-interpolated data as shown in Fig. 4b. Retardation of the fatigue crack predominantly occurs inside the grains. Grain boundary effect on the crack growth rate is less pronounced. Mechanism responsible for the fatigue crack retardation in the studied ferritic stainless

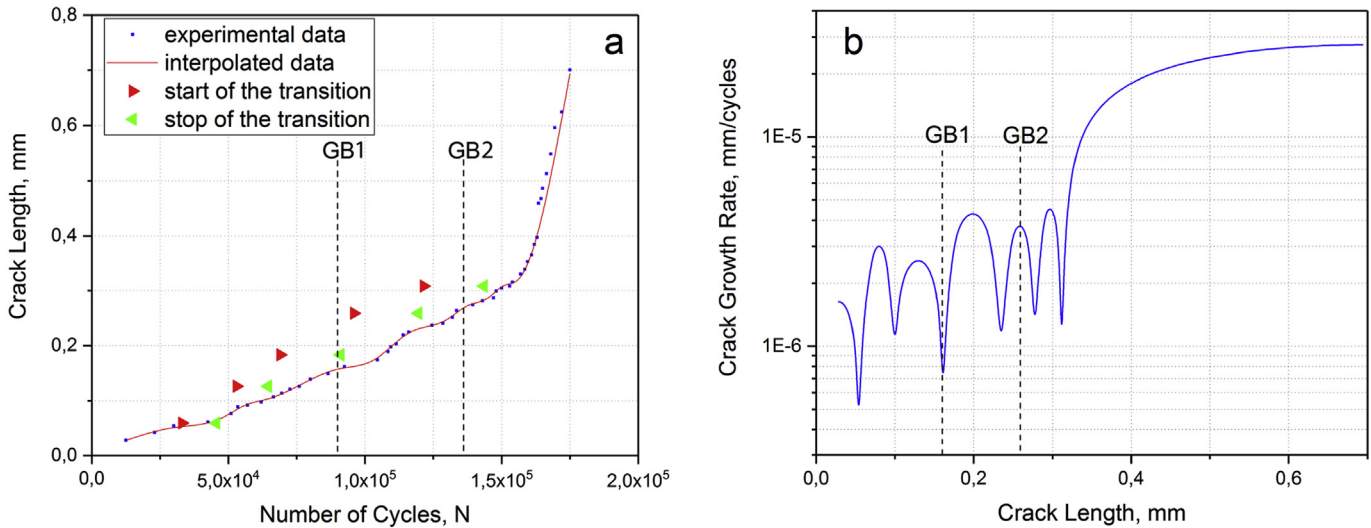


Fig. 4. Relationship between crack length vs. number of cycles (a) and crack growth rate vs. crack length (b) for a ferritic stainless steel specimen tested in fatigue.

steel was investigated by DIC analysis and SEM fractography.

3.1. DIC analysis

Strain field was calculated by DIC and visualized as shown in Fig. 5a and b. Linear deformations both parallel and normal to the loading direction (E_{yy} and E_{xx} , respectively) represent pairs of highly tensioned and compressed areas, which appear simultaneously as the fatigue crack propagates. Such a behavior manifests the presence of shear deformation that was found to be highly localized inside the grains on the crack path while the macroscopic deformation is small. A number of specimens of the studied steel tested in the same conditions show the similar behavior of plasticity accumulation.

Linear profiles of the maximum shear strain were measured from each point of the deformation maxima over all fatigue test frames as shown in Fig. 5b. Data were combined by plotting a 3D profile, where the maximum shear deformation is plotted versus the number of cycles and the profile length (see example in Fig. 6). The observed 3D profiles of the maximum shear strain reveal almost no deformation at the beginning of the fatigue test. At

certain number of fatigue cycle intervals the shear deformation increases steeply, but the area subjected to deformation remains localized during all the fatigue tests. Insert of Fig. 6 summarizes the results of measurement of the maximum shear strain from all the observed strain localization zones analyzed over the fatigue test. The observed transitional stages consequentially start from the fatigue cycle where the previous transition was completed. After the transitional stage is completed the following increase of the deformation is caused apparently by crack opening. The transition starts and stops with respect to the crack growth propagation as presented in Fig. 4a. Worth to note is that a starting point of transition was observed even up to 100 μm ahead of the crack tip that is significant in comparison to actual crack size.

The observed transition behavior correlates well with the retardation periods of the fatigue crack growth shown in Fig. 4. Distances from the notch tip to the maxima of the shear strain localization were measured and plotted versus the number of cycles associated with start and stop of the transitional stages. Within the first grain the crack growth retardation starts almost together with the localization of the shear strain and changes to the crack acceleration as soon as the transition is completed. As the fatigue

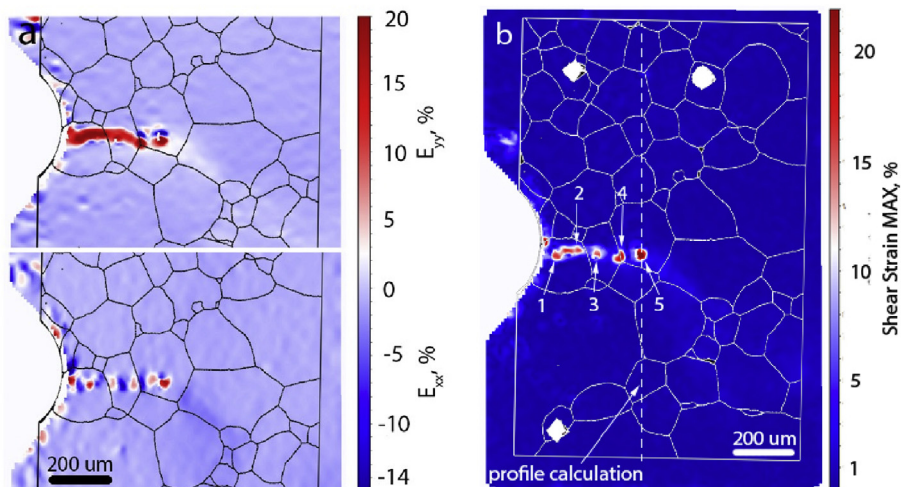


Fig. 5. Strain field of the linear deformations E_{xx} and E_{yy} (a) and MAX shear deformation (b) calculated by DIC during a fatigue test of the ferritic stainless steel specimen.

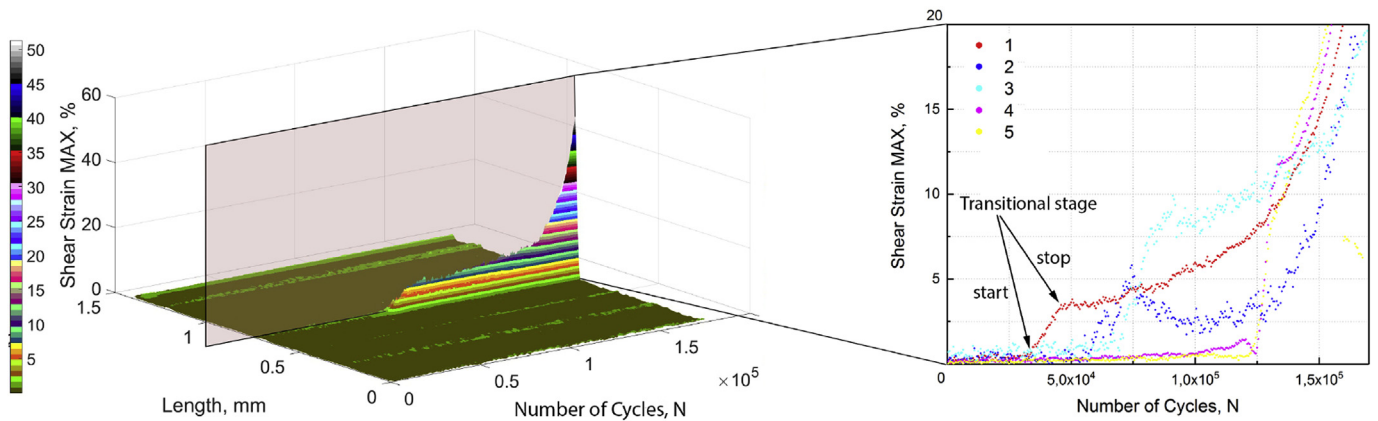


Fig. 6. Linear profile of the shear strain localization areas measured during the fatigue test of the ferritic stainless steel specimen. Data of the maximum shear strain calculated for each strain localization point are summarized in the insert.

crack propagates the shear strain localization zones form before the crack retardation ahead of the crack tip.

The maximum resolved cumulative shear strain of each localized zone was calculated at the end of the transition periods and is summarized in Table 2 regarding the grain orientation. Schmid factor was calculated for the grains containing the strain-localized areas according to the most preferable slip planes in bcc crystal: {110}, {112} and {123} (see Fig. 7).

The cumulative maximum shear strain increases slightly with crack traversing from the first to the following grain, but the increase is controlled, apparently, by the change in stress conditions due to the reduction of the cross-section area of the specimen rather than by the orientation of the grains. However, shear strain intensity factor calculated as quotient between cumulative maximum shear strain and deformation area reveals a significant increase of shear strain localization in the second grain of the smallest Schmid factor, while the shear localization on the GB is smallest. Worth to note is that fatigue crack propagates across the GBs of low misorientation angle. The angles of misorientation of about 15° and 20° are associated with GB1 and GB2, respectively. GB misorientation and their distribution were defined from EBSD maps obtained in the vicinity of the notch of the specimen and are presented in Fig. 8a.

3.2. Fractography

The transgranular fatigue fracture surface is macroscopically brittle as shown in Fig. 9. The fatigue fracture starts from the pre-cracking zone which width varies from 20 μm to about 1 μm (see Fig. 9 b). Different loading conditions of the pre-cracking procedure and the fatigue testing result in a different fracture surface appearance. While the pre-cracked zone shows almost a flat fracture, the following fracture surface represents a number of important features, which shed light on the fatigue crack propagation behavior.

Fracture surface was studied in the vicinity of the side surface of the specimen subjected to the DIC analysis. The higher magnification reveals the fatigue striations formed as ripples on the facets of the river patterns (see Fig. 9 b). Formation of the fatigue striations is associated usually with Stage II of the fatigue crack growth [1]. However, the Stage II was found to be changed to Stage I of the crack propagation in the direction of the primary slip system causing the formation of cleavage-like faceted or serrated fracture surface as shown in Fig. 10. Centers of the shear strain localization zones are marked by numbers in Fig. 10. Fracture surface associated with Stage I crack growth forms apparently in the area subjected to compression strain in direction normal to the applied load (see Fig. 5a). Worth to note is that the crack length when its retardation occurs, is associated well with the location of Stage I microscopic fracture shown in Fig. 10.

Fractography was studied evidencing the formation of faceted fracture surfaces close to the side surface as well as in the interior of the specimen. Fig. 9 c shows a fractograph obtained from the interior in the vicinity of the notch. Fatigue crack propagated through the material forming a river pattern morphology. Direction of the observed river pattern corresponds to the direction of the microscopic fatigue crack path. Many parallel straight lines forming normal to the river pattern direction are observed on the fracture surface and associated apparently with crack propagation by <111> pencil-glide slip. Worth to note is that the faceted fracture surface formed in the vicinity of the notch. The characteristic length of the zone containing the faceted fracture surface is about 300 μm that correlates well with the average grain size of the studied steel. Further growth of the fatigue crack results in formation of a rough fracture surface which is caused apparently by high deformation plastic zone forming ahead of the fatigue crack tip.

In order to exclude the possible effect of non-metallic inclusions (NMI) on the fatigue crack growth retardation fracture surface of the specimen was studied by QBSD back-scatter electron detector, which is good for compositional contrast imaging (see Fig. 11). NMIs

Table 2

Parameters of the accumulated strain. Maximum Schmid factor of the grains containing the strain-localized areas are marked by bold.

Localization point No.	Grain No.	Deformation area, mm ²	Cumulative maximum shear strain, %	Shear strain intensity factor	Schmid factor		
					{110}	{112}	{123}
1	1	0.0302	0.65	21	0.43	0.5	0.49
2		0.0048	0.55	114			
3	2	0.0012	0.72	600	0.35	0.41	0.39
4	GB2	0.0437	0.52	11	GB2		
5	3	0.0075	1.16	154	0.45	0.48	0.49

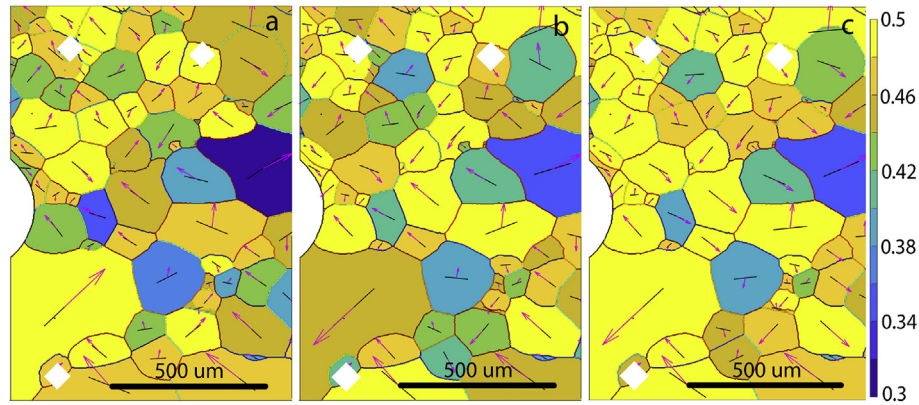


Fig. 7. Schmid factor analysis for {110} (a), {112} (b) and {123} (c) slip planes of the side surface of the specimen in the vicinity of the notch before fatigue testing. Black lines and red arrows show the active slip planes and slip directions, respectively. Calculated by MTEX software.

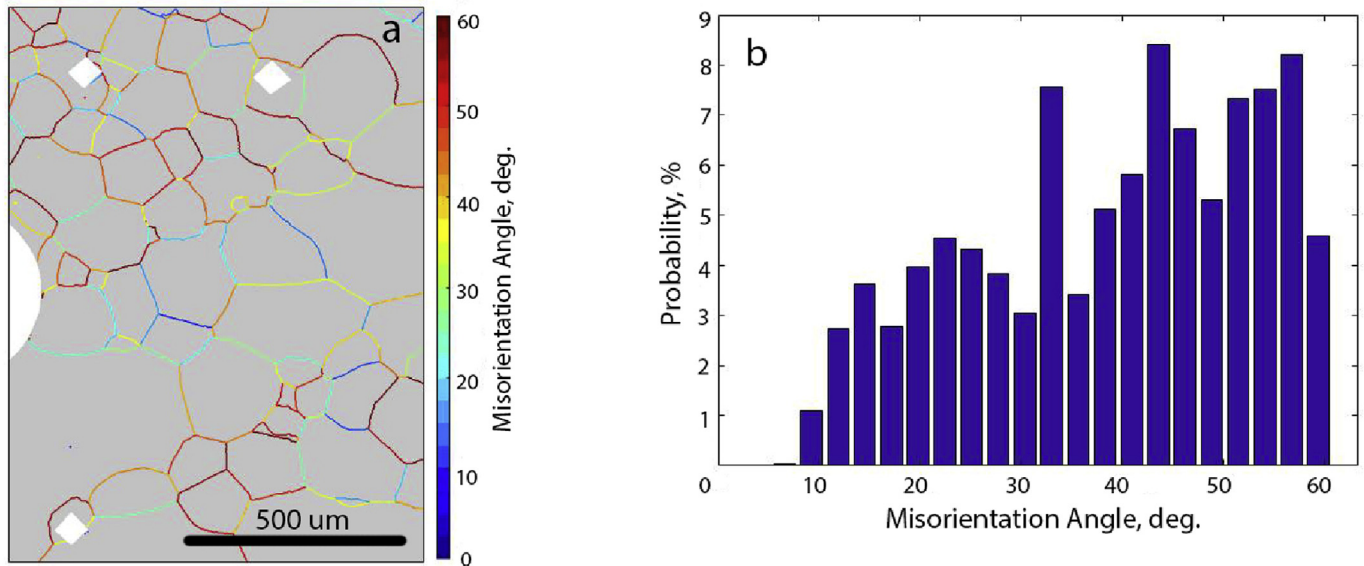


Fig. 8. GB misorientation analysis from EBSD map of the studied steel in the vicinity of the notch (a) and calculated GB misorientation angle distribution (b).

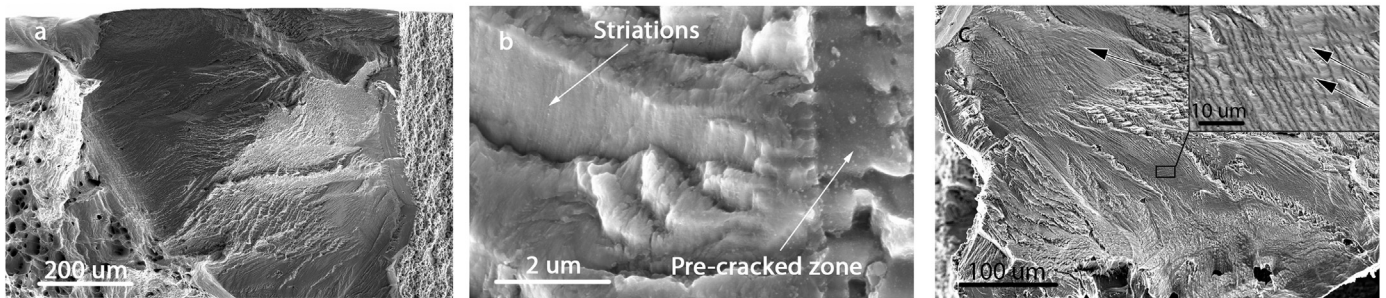


Fig. 9. Fractography of the ferritic stainless steel specimen tested in fatigue: general view of the fracture surface (a), higher magnification of the fatigue crack initiation zone (b) and fractograph obtained from the interior of the specimen in the vicinity of the notch (c) (Black arrows of Fig. 9c show the faceted fracture surface. Insert shows higher magnification of faceted fracture surface).

were observed only in the vicinity of the fifth strain localization area. These NMIs may have affected the crack growth rate, but since the fatigue crack growth retardation was observed also in areas free of NMIs, the effect of NMIs on fatigue crack growth rate is very unlikely.

4. Discussion

Stage I of the fatigue crack growth is usually associated with a slow crack growth rate, where the increment of the average crack extension is less than 10^{-6} mm/cycle [22]. In this regime, the stress

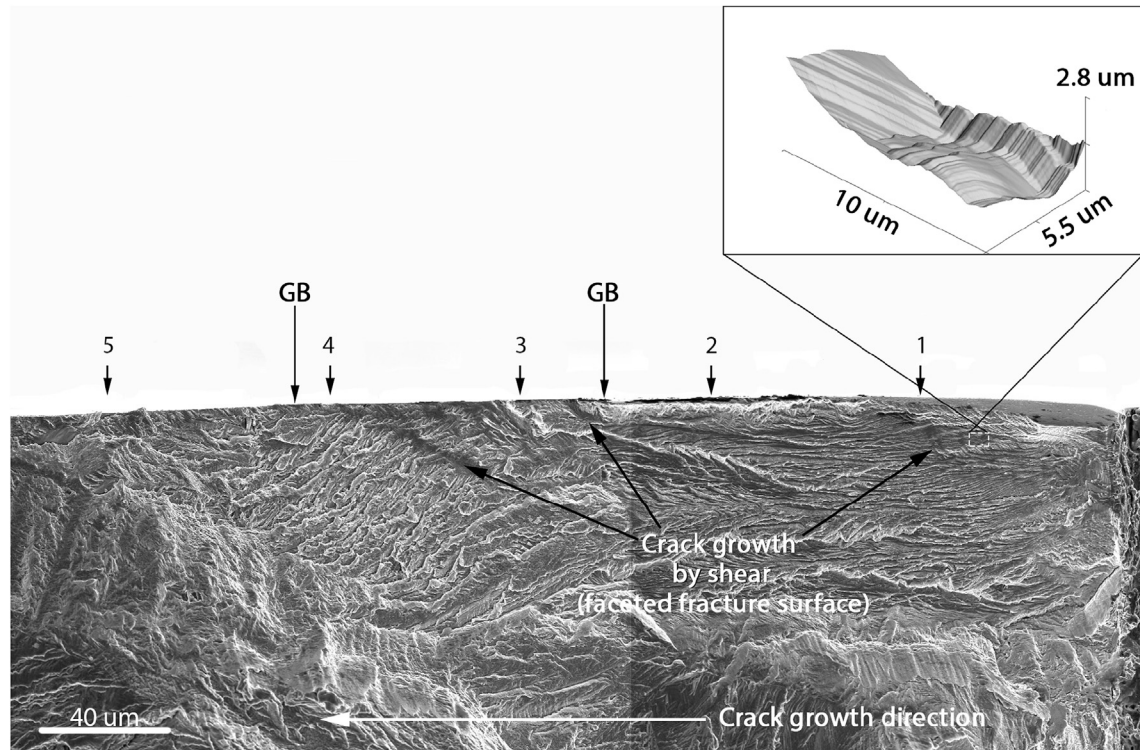


Fig. 10. Micrograph of the fracture surface in the vicinity of the notch. AFM image of persistent slip bands formed on the fracture surface of the specimen in both Stage I and Stage II fracture mode is shown in the insert.

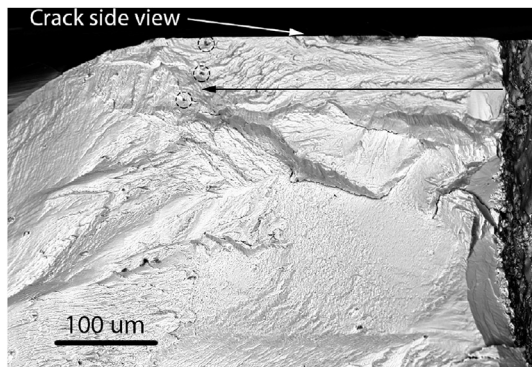


Fig. 11. Compositional contrast imaging of the fracture surface of the specimen. Arrow shows the location of the fifth local retardation event. NMIs are marked by circles.

intensity factor range approaches the fatigue crack growth threshold value for transition of the crack growth rate to the mid-growth rate following the so-called Paris relation [22]. The Paris regime is associated with Stage II mechanism of the large crack propagation. As shown earlier by Tokaji et al. Stage II regime is related also to mechanically small crack growth, which is slightly affected by microstructure and has an anomalous (rapid) propagation behavior different from that of Paris regime [16]. This behavior correlates well with the data of crack growth rate shown in Fig. 4 b and confirms the threshold character of the observed fatigue crack growth between Stage I and II, but does not correspond to the transition between small and large fatigue crack growth. In previous studies, Taylor and Knott [23,24] have suggested that transition between the small fatigue crack with anomalous crack growth behavior and large fatigue crack takes place at the crack length of $10d$, where d is microstructural unit size

associated usually with the average grain size. In the present study, the maximum crack length is less than two times of the average grain size.

The existence of the fatigue crack growth threshold region was first proposed by McClintock, when he postulated that the fatigue crack growth may cease to advance when a critical value of local accumulated strain over a certain characteristic distance ahead of the crack tip reaches a critical value [22,25]. The proposed model fits well with the observation where the crack growth rate decreases shortly as it approaches the shear strain localization zone (see Fig. 4a). However, the size of the damage zones is not compatible with the characteristic microstructural size scale (grain size) and depends apparently on the crystal orientation. The characteristic sizes of the shear deformation areas measured from the shear strain field profiles are presented in Table 2. Worth to note is that the grain with the smallest Schmid factor suffers from the highest localization of the shear deformation or accumulated strain intensity, while the smallest strain intensity is on the grain boundary. Thus, one can conclude from Figs. 5 and 10, that the deformation processes apparently control the small fatigue crack growth rather than GBs. However, the situation may change with the increase of the GB misorientation angle. Even though the small crack growth retardation events do not correlate always with GB positions, the GBs are generally considered as the main reason for the small crack retardation [16,26–28]. Recent study performed by Hansson et al. [29] using a dislocation formulation in the boundary element approach shows, however, that the high-angle grain boundaries do not affect the crack growth rate, while the low-angle grain boundaries can result in both an increase and decrease of the crack growth rate. According to the present study, we conclude that the major part of the retardation events can be associated with the highly localized deformation ahead of the crack tip.

The details of the fracture surface of Stage I crack growth were

studied by AFM as shown in the insert of Fig. 10. Crack growth along shear bands emanating from the crack tip results in formation of the facets, which are not totally flat but contain a number of dislocation slip line offsets or persistent slip bands (PSB) formed as a result of the high cyclic slip activity. The similar behavior of the small fatigue crack propagation with two different crack growth mechanisms was observed also in face-centered cubic crystal structure of Inconel 718 alloy, where striations were found in a few grains, while the crack growth was dominated by the slip-based mechanism [12]. Andersson et al. [12] postulated that the different crack growth mechanisms seem to be active if the slip planes at the crack tip are far from 45° to the applied load direction that corresponds to the lower Schmid factor or at low stress intensity factor range levels where few slip systems are operative. The assumption correlates well with the results obtained for the studied ferritic stainless steel. However, the variation of the crack growth mechanisms in the studied steel was observed within the grains associated not only with grain orientation but also with the plastic deformation. The intensity of the plastic shear deformation ahead of the crack tip affects the mechanism of the small fatigue crack propagation, its deflection and retardation.

Based on the current results for the studied ferritic stainless steel, a schematic illustration of the microstructurally small fatigue crack propagation is shown in Fig. 12 including both Stage I and II mechanisms. Stage II fatigue crack propagates by formation of dislocation cell structures and their breakdown by PSBs at the crack tip. Crack growth changes to single slip mechanism (Stage I) as soon as the crack tip approaches the shear strain localization area. Local shear strain accumulating ahead of the fatigue crack tip results in a variation of fatigue crack growth mechanism as shown in Fig. 12a and b and c. Such a variation of the crack propagation mechanism is accompanied with crack growth rate retardation. The fatigue crack

growth rate increases after the crack tip approaches a middle point of the shear strain localization area. Such a behavior of the fatigue crack propagation characterizes both the near-surface and interior fatigue fracture in the studied ferritic stainless steel. In the previous studies, the primary mechanism responsible for the crack growth rate retardation in the presence of plastic deformation is usually plasticity-induced crack closure [30,31]. Since the observed shear deformation zones form in the material ahead of the fatigue crack causing propagation retardation (see Fig. 4a) and the size of the deformation area is much smaller than that proposed by Elber et al. [21,22], the mechanism of plasticity-induced crack closure does not explain the observed small fatigue crack growth behavior. The effect of neighboring grains and GBs locating in the cross-section of the specimen on the strain localization needs, however, further investigation.

Small fatigue crack propagation in the studied ferritic stainless steel is accompanied by the formation of a number of local plastic deformation zones ahead of the crack tip. Some evidences of the local plasticity that do not correspond to the linear elastic fracture mechanics were already shown for coarse-grained 3% silicon iron, where the plastic zone ahead of the crack tip was estimated from slip displacement [13]. In the previous studies the crack retardation and arrest were associated mainly with grain boundaries [25,27,28]. The most recent researches show that the small fatigue crack retardation, arrest or acceleration may be caused by low-angle grain boundaries formed because of the emitted dislocation lines from the crack tip [8,9]. The discrete dislocation mechanism does not explain, however, the formation of the intermittent strain localization zones observed in the studied steel. Most likely a combined mechanism of continuum mechanics and discrete dislocation mechanisms can better describe the distinct nature of plasticity [10].

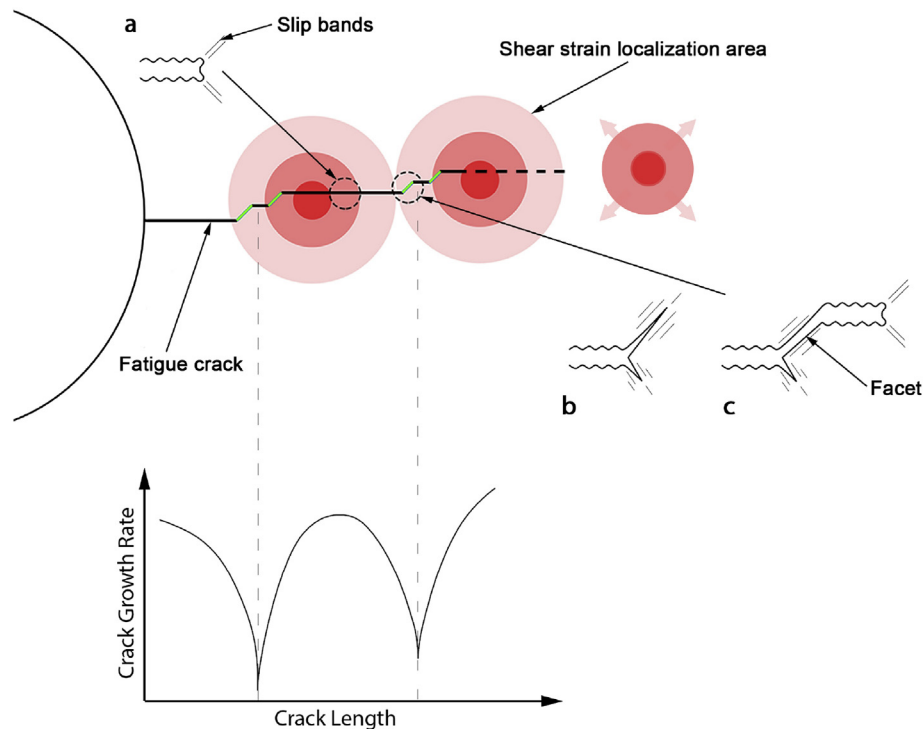


Fig. 12. Behavior of a small fatigue crack growth in a bcc ferritic steel (ASTM UNS S43940 ferritic stainless steel). Fatigue crack growth by Stage II multiple-slip mechanism is shown by black line and fatigue crack growth by Stage I single-slip mechanism by green line, respectively. After crack tip approaches the shear strain localization area the Stage II fatigue crack growth mechanism (a) changes intermittently to Stage I (b, c) forming a faceted profile. The intermittent change of the crack growth mechanism accompanied with fatigue crack growth rate retardation is shown schematically on the crack growth rate diagram.

5. Conclusions

DIC analysis evidences the intermittent appearance of the shear strain localization zones ahead of the crack tip as the fatigue crack propagates. The fatigue crack growth rate is affected by the accumulated shear deformation areas rather than by microstructural features such as grain boundaries. The relationship between the grain orientation (Schmid factor) and the shear strain intensity factor is inversely proportional.

Fatigue crack propagates transgranularly. The small fatigue crack grows by formation of both striations and flat facets associated with cracking by high single shear stress/strain in the direction of the primary slip system. Crack propagation by single shear mechanism takes place in the areas where the material is subjected to compression in the direction normal to the applied loading direction. The crack growth occurs predominantly by the single shear mechanism in the direction of the primary slip system, when a critical shear strain ahead of the crack tip is reached.

Acknowledgements

The ASTM UNS S43940 ferritic stainless steel was provided by Outokumpu Stainless Oyj. Research was partly supported by Aalto University. The research is related to the Academy of Finland project number 298762.

References

- [1] P.J.E. Forsyth, A two stage process of fatigue crack growth, Proc. Cranfield Symposium, Lond. (1962) 76–94.
- [2] B. Tomkins, W.D. Biggs, Low endurance fatigue in metals and polymers, J. Mat. Sci. 4 (1969) 544–553.
- [3] P. Neumann, New experiments concerning the slip processes at propagating fatigue cracks - I, Acta Metall. 22 (1974) 1155–1165.
- [4] H. Vehoff, P. Neumann, In situ SEM experiments concerning the mechanism of ductile crack growth, Acta Metall. 27 (1979) 915–920.
- [5] P. Peralta, C. Laird, Fatigue fracture at bicrystal interfaces: experiment and theory, Acta Mat. 46 (6) (1998) 2001–2020.
- [6] C. Laird, Influence of metallurgical structure on the mechanisms of fatigue crack propagation, Fatigue Crack. Propag. ASTM-STP 415 (1967) 131–180.
- [7] P. Paris, F. Erdogan, Critical analysis of crack propagation laws, J. Basic Eng. 85 (4) (1963) 528–533.
- [8] C. Bjerken, S. Melin, Influence of low-angle grain boundaries on short fatigue crack growth studied by a discrete dislocation method, in: Proceedings of the 17th European Conference Fracture, VUTIUM Brno, Czech Republic, 2–5 September, 2008.
- [9] C. Bjerken, S. Melin, Growth of a short fatigue crack – a long term simulation using a dislocation technique, Int. J. Solids Struct. 46 (2009) 1196–1204.
- [10] F.O. Riemelmoser, R. Pippan, O. Kolednik, Cyclic crack growth in elastic plastic solids: a description in terms of dislocation theory, Comput. Mech. 20 (1997) 139–144.
- [11] P. Hansson, S. Melin, Dislocation modelling of short fatigue crack growth through alternating slip, in: In Proceedings of 15th European Conference Fracture, August 11–13, 2004.
- [12] H. Andersson, C. Persson, In-situ SEM study of fatigue crack growth behavior in IN718, Int. J. Fatigue 26 (2004) 211–219.
- [13] M. Jono, A. Sugeta, Y. Uematsu, Atomic force microscopy and the mechanism of fatigue crack growth, Fatigue & Fract. Eng. Mater. Struct. 24 (2001) 831–842.
- [14] K. Tokaji, T. Ogawa, Y. Harada, Evaluation on limitation of linear elastic fracture mechanics for small fatigue crack growth, Fatigue & Fract. Eng. Mater. Struct. 10 (1987) 281–289.
- [15] K. Tokaji, T. Ogawa, S. Osako, Y. Harada, The growth behaviour of small fatigue cracks; the effect of microstructure and crack closure, Fatigue 2 (1987) 313–322.
- [16] K. Tokaji, T. Ogawa, Short Fatigue Cracks,ESIS 13, in: K.J. Miller, E.R. de los Rios (Eds.), The Growth Behavior of Microstructurally Small Fatigue Cracks in Metals, Mechanical Engineering Publications, London, 1992, pp. 85–89.
- [17] P. Peralta, S.-H. Choi, J. Gee, Experimental quantification of the plastic blunting process for stage II fatigue crack growth in one-phase metallic material, Int. J. Plasticity 23 (2007) 1763–1795.
- [18] J.D. Carroll, W. Abuzaid, J. Lambros, H. Sehitoglu, High resolution digital image correlation measurements of strain accumulation in fatigue crack growth, Int. J. Fatigue 57 (2013) 140–150.
- [19] ASTM-E1382-97, Standard test methods for determining average grain size using semiautomatic and automatic image analysis, West Conshohocken (PA) ASTM Int. (2004), <https://doi.org/10.1520/E1382-97R04>.
- [20] E. Malitckii, Y. Yagodzinsky, P. Lehto, H. Remes, J. Romu, H. Hanninen, Hydrogen effects on mechanical properties of 18%Cr ferritic stainless steel, Material Sci. Eng. A 700 (2017) 331–337.
- [21] S. Bossuyt, Optimized patterns for digital image correlation, in: Proceedings of the 2012 Annual Conference on Experimental and Applied Mechanics, Imaging Methods for Novel Materials and Challenging Applications, vol. 3, 2013, pp. 239–248.
- [22] S. Suresh, Fatigue of Materials, second ed., 1998, ISBN 0521578477. Cambridge.
- [23] D. Taylor, J.F. Knott, Fatigue crack propagation behavior of short cracks: the effect of microstructure, Fatigue & Fract. Eng. Mater. Struct. 4 (1981) 147–155.
- [24] D. Taylor, in: K.J. Miller, E.R. de los Rios (Eds.), “Fatigue of Short Cracks: the Limitation of Fracture Mechanics”, the Behavior of Short Fatigue Cracks, Mechanical Engineering Publications, London, 1986, pp. 479–490.
- [25] F.A. McClintock, On the plasticity of the growth of fatigue cracks, Fract. Solids 20 (1963) 65–102.
- [26] V. Doquet, Micromechanical simulations of microstructure-sensitive stage I fatigue crack growth, Fatigue & Fract. Eng. Mater. Struct. 22 (1998) 215–223.
- [27] S.M. Ohr, An electron microscope study of crack tip deformation and its impact on the dislocation theory of fracture, Mater. Sci. Eng. 72 (1985) 1–35.
- [28] Z. Shen, R.H. Wagoner, W.A.T. Clark, Dislocation and grain boundary interactions in metals, Acta Metall. 36 (1988) 3231–3242.
- [29] P. Hansson, S. Melin, Grain boundary influence on short fatigue crack growth rate, Int. J. Fract. 165 (2010) 199–210.
- [30] W. Elber, Fatigue crack closure under cyclic tension, Eng. Fract. Mech. 2 (1970) 37–45.
- [31] W. Elber, The significance of fatigue crack closure, Damage Toler. Aircr. Struct. 486 (1971) 230–242.